## Introduction

Amyloid-beta (Aβ) peptide deposition in senile plaques (SPs, for plaque terminology see 'Methods' section), and the formation of neurofibrillary tangles (NFTs) from tau are the key histopathological features for the diagnosis of Alzheimer's disease (AD) (Mott and Hulette, 2005). Great efforts are currently underway to define reliable biomarkers to establish the diagnosis of AD *intra vitam* and in early disease phases, a prerequisite for the development of disease-modifying therapies.

Amyloid is a generic term used to describe polypeptide filaments that are folded into a cross β-sheet structure and as a consequence bind dyes such as Congo Red and the Thioflavins S and T (Lockhart, 2006). Both Aβ, which forms the fibrils variably associated with SPs (and cerebrovascular amyloid), and tau, which forms the paired helical and straight filaments associated with NFTs, are types of amyloid (Serpell, 2000; Berriman *et al.*, 2003; Barghorn *et al.*, 2004). [11C]-PIB is one of a number of positron emission tomography (PET) imaging probes that were derived from

Thioflavin T and the radiotracer is thought to selectively bind to the highly fibrillar (i.e. amyloid rich) SP subtype known as classical plaques (CPs) (Mathis *et al.*, 2004).

In support of this premise a series of reports have demonstrated the increased, region specific, retention of [11C]-PIB in clinically diagnosed AD patients compared with non-demented control groups (Klunk *et al.*, 2004; Verhoeff *et al.*, 2004; Archer *et al.*, 2006; Engler *et al.*, 2006; Fagan *et al.*, 2006; Edison *et al.*, 2007) in a pattern that broadly matches CP distribution (Nordberg, 2004). Additionally, an inverse correlation of PIB retention with the pattern of decreased regional cerebral glucose metabolism rate (rCMRglc) has been observed (Klunk *et al.*, 2004; Buckner *et al.*, 2005; Engler *et al.*, 2006; Edison *et al.*, 2007). Finally, a 2-year-follow-up study on a cohort of AD patients indicated that the amyloid load, as measured by [11C]-PIB, remained stable irrespective of clinical progression determined by both cognitive measures and rCMRglc (Engler *et al.*, 2006). These latter two findings in particular suggest that amyloid deposition, as detected by PIB, is an early event in the pathogenesis of AD that may (i) precede a decline in cognitive function and (ii) reach an early plateau which then remains stable.

However, reconciling these global, *in vivo* observations with data from both the large number of antecedent post-mortem studies detailing the regional, microscopic spread of AD pathology (Braak and Braak, 1991*a*; Berg *et al.*, 1998; Price and Morris, 1999) and the relatively sparse literature characterizing the interaction of imaging probes with amyloid lesions (Lockhart, 2006) highlights a number of important discrepancies. First, the high retention of [11C]-PIB in brain regions not normally associated with a high CP load such as the striatum and frontal cortex (Klunk *et al.*, 2004; Nordberg, 2004; Buckner *et al.*, 2005; Engler *et al.*, 2006; Edison *et al.*, 2007) cannot readily be explained by the reported specificity of PIB for CPs. For example studies have demonstrated that the vast majority of plaques in the striatum are of a diffuse plaque (DP) type (Wisniewski *et al.*, 1989; Suenaga *et al.*, 1990) and that CPs are not a dominant pathological feature of the frontal cortex during the early stages of AD (Mochizuki *et al.*, 1996; Berg *et al.*, 1998; Price and Morris, 1999). However, the findings associated with this latter observation are not universal (Braak and Braak, 1991*a*; Markesbery *et al.*, 2006). Secondly, the dichotomy of the ligand retention pattern into essentially 'PIB-positive' or 'PIB-negative' is at odds both with the central role of the CP in disease progression (Selkoe and Schenk, 2003). A number of studies have also demonstrated that CPs begin to form near the time of clinical presentation and then increase with disease severity (Braak and Braak, 1991*a*; Berg *et al.*, 1998; Price and Morris, 1999). Thirdly, a 'pathologic' or 'PIB-positive' retention pattern has also been identified in 22 to 40% of cognitively normal individuals (Fagan *et al.*, 2006; Mintun *et al.*, 2006; Rowe *et al.*, 2007) and this represents a significant false positive rate. As no longitudinal PIB-PET data is available from these cognitively normal subjects, it is currently unclear whether these findings reflect the molecular development of prodomal AD (Barnes *et al.*, 2006) or are consistent normal ageing. Finally, only one imaging study to date has considered the potential influence of the apolipoprotein E (ApoE)-ε4 allele on the pattern of PIB retention (Rowe *et al.*, 2007), as this variant is linked with an earlier disease onset, a more rapid cognitive decline, and a more pronounced accumulation of both SPs and cerebrovascular amyloid angiopathy (CAA) (Berg *et al.*, 1998; Attems, 2005). These issues are further exemplified by the application of [11C]-PIB in non-AD patient populations such as dementia with Lewy bodies (DLB) and frontotemporal dementia (FTD) (Bacskai *et al.*, 2007; Rowe *et al.*, 2007; Rabinovici *et al.*, 2007).

In order to address these important knowledge gaps an autoradiography study was undertaken using a tritium labelled preparation of the PIB ([3H]-PIB) and fresh-frozen brain sections from cases containing AD-associated neuropathological lesions (SPs, CAA and NFTs). Importantly the study utilized subjects of known ApoE genotype, a tracer concentration of radioligand relevant to imaging studies (Mathis *et al.*, 2004; Rowe *et al.*, 2007) and histological examination of adjacent sections, so that radiolabelled features could be positively linked to specific lesions.

## Methods

### Compounds

Tritiated Pittsburgh Compound-B ([3H]-PIB, *N*-methyl-[3H]2-(4′-methylaminophenyl)-6-hydroxybenzothiazole was prepared as a custom synthesis by GE Healthcare UK Ltd (Little Chalfont, UK) at a specific activity 71 Ci/mmol (2.63 TBq/mmol). BTA-1, 2-(4′-methylaminophenyl)benzothiazole (Sigma, Poole, UK) was prepared as a 10 mM stock in dimethylsulphoxide and stored at −20°C.

### Preparation of cryosections

Fresh, frozen brain tissues were obtained from the Brain Donation Program at Sun Health Research Institute (Sun City, AZ, USA). Four consecutive cryosections (8–10 μm thickness) were prepared from each brain specimen and mounted onto statically charged ('plus') glass slides prior to airtight storage with desiccants at −80°C. The first and third sections in each series were used for histochemical analysis. The second and the fourth sections were used for radioligand binding studies defining the total ([3H]-PIB) and non-displaceable binding (NDB) ([3H]-PIB plus BTA-1) signals, respectively.

### Radiolabelling of sections

Slides were thawed for 10 min at room temperature (25°C) prior to incubation in PBS/E buffer [phosphate buffer saline (PBS) containing 10% v/v ethanol, pH 7.2] for 15 min at room temperature. Slides were then incubated with 0.5 nM [3H]-PIB (total binding) or 0.5 nM [3H]-PIB plus 10 μM BTA-1 (NDB) for 60 min at room temperature and then terminated by consecutive 30 s incubations in PBS/E (×2) and distilled water (all at 4°C). Slides were dried under a cold air stream and then apposed with Hyperfilm-3H (GE/Amersham, RPN535B: early availability batch).

**Table 1** Summary of histological and immunohistological staining techniques used to identify neuropathological lesions

| | Aβ immunostain (6E10) | Thioflavin S | Gallyas |
|---|---|---|---|
| CPs | ++ | ++ | N/A |
| DPs | +, +/− | +/− | N/A |
| CAA | ++ | ++ | N/A |
| NFTs | N/A | ++ | ++ |

*Note*: As noted in the 'Methods' section both the morphology and differential staining intensity (++ strong staining, + moderate staining, +/− weak staining, N/A not applicable) were used to distinguish between lesion types.

## Film development and analysis

Films were developed after an 8-week exposure using GBX developer solutions (Kodak, New Haven, USA). Images of the autoradiographs were captured using the MCID digital densitometry system (Interfocus, Linton, UK). No manipulations other than optimization of lighting conditions (for image capture), image cropping and re-sizing were performed.

## Nomenclature and classification of pathological features

The identification of SPs, CAA and NFTs was based on data from two separate staining techniques (Table 1) as well as morphological appearance. The terminology for SP phenotypes follows that of Berg *et al.* (1998). Plaques with generally spherical shapes displaying strong staining with both Thioflavin S and the anti-Aβ monoclonal antibody 6E10 were defined as classical plaques (CPs). CPs were not further differentiated into neuritic and cored plaques. Plaques with spherical or irregular shapes displaying weak staining for Thioflavin S and weak-to-moderate staining with 6E10 were defined as diffuse plaques (DPs). Senile plaques (SPs) are used as a generic term to encompass both types of plaque lesions (i.e. CPs and DPs). CAA was identified on the basis of strong staining with 6E10 and Thioflavin S, and was differentiated from CPs on the basis of morphological appearance. NFTs were identified by Gallyas and Thioflavin S staining.

## Histochemical procedures

All procedures were performed at room temperature unless otherwise noted.

### *Thioflavin S staining*

Thioflavin S is a stain used to detect lesions containing high amounts of amyloid structures and will primarily label CPs, CAA and NFTs (Dickson, 2005). DPs contain low amounts of amyloid structure and only stain weakly with this dye (Dickson, 2005). Sections were removed from the freezer and immediately immersed for 30 min in 4% formaldehyde, freshly prepared from paraformaldehyde crystals and buffered to pH 7.4. Following washes in PBS and partial drying at room temperature, the sections were defatted in 1:1 chloroform/ethanol for 1 h, washed briefly twice in 100% ethanol and then hydrated through graded alcohols to water. Sections were then stained in 0.1% Thioflavine S for 10 min, differentiated rapidly in 80% ethanol and cover-slipped with Apathy's medium.

### *Immunohistochemical staining for Aβ peptide using 6E10*

The anti-Aβ monoclonal antibody 6E10 is considered a sensitive marker for CPs and CAA, but may stain diffuse deposits less intensely (Dickson, 2005). Washes were performed between all steps with PBS containing 0.1% Triton X-100. Sections were removed from the freezer and immediately immersed in 70% ethanol for 2 min. Endogenous peroxidase was then suppressed by immersion in 1% hydrogen peroxide for 30 min. After additional washes, sections were incubated overnight in 6E10 (CHEMICON International, Temecula, USA) diluted 1:1000 and detected using VECTASTAIN Elite ABC Kit (Vector Laboratories, Burlingame, USA), dehydrated and mounted in Permount (Fisher Scientific, Fair Lawn, USA).

### *Gallyas staining*

The Gallyas method is a silver-staining technique that in this form is considered specific for NFTs (Braak and Braak, 1991b; Dickson, 2005). Sections were removed from the freezer and fixed as described earlier for Thioflavin S staining. The staining protocol was as described (Braak and Braak, 1991b) with the addition of two pre-treatment steps to minimize non-specific red blood cell staining. These consisted of immersion in 0.25% potassium permanganate for 4 min followed by incubation in 5% oxalic acid for 5 min.

## Results

The neuropathological lesions under investigation were studied using four different brain regions: Category A, SP-predominant pathology used mid-frontal gyrus (MFG); Category B, Mixed pathology (DPs, CPs, CAA and NFTs) used superior parietal lobe (SPL); Category C, CAA-predominant pathology used occipital lobe (OCL); and Category D, NFT-predominant pathology used entorhinal cortex (ECX). The neuropathological sections under investigation were pre-selected for the presence of the desired neuropathological lesions and were as far as possible derived from cases with pathologically confirmed AD. However, given the considerable intermingling of lesion types in AD cases and a desire to sample each lesion type in a relatively pure form it was necessary to use additional neuropathological disease groups. A total of 16 cases (four per category) were analysed in the study and representative data from two cases from each category A–D are reported here in detail (Table 2). A full listing of all 16 cases is provided in the supplementary data.

## Category A sections (SP-predominant pathology)

The interaction of [3H]-PIB (0.5 nM) with relatively pure populations of SPs (i.e. a mixture of DPs and CPs) was investigated using sections from the MFG of cases with

**Table 2** Neuropathological characteristics of sections

| Case | Brain region | Pathology scores of sections used in study DP | CP | NFT | CAA | ApoE status | CAA-NDB | Neuropathological diagnosis |
|---|---|---|---|---|---|---|---|---|
| A1 | MFG | +++ | ++ | – | – | 4/4 | N.A.* | Probable AD |
| A2 | MFG | +++ | + | – | + | 3/4 | Yes | Probable AD |
| B1 | SPL | +++ | +++ | + | +++ | 4/4 | Yes | Definite AD |
| B2 | SPL | +++ | +++ | + | ++ | 4/4 | Yes | Definite AD |
| C1 | OCL | ++ | ++ | – | ++ | 2/3 | No | Possible AD |
| C2 | OCL | – | – | – | +++ | 4/4 | Yes | Probable AD |
| D1 | ECX | – | – | +++ | – | 2/3 | N.A.* | Not AD |
| D2 | ECX | – | – | + | – | –/– | N.A.* | Not AD |

*Note*: Pathology scores: +++, frequent. ++, moderate. +, sparse. –, absent. Note that the neuropathological diagnosis for each case was based on a full pathological examination according to Consortium to Establish a Registry for AD criteria (Mirra *et al.*, 1991). Note that no ApoE genotyping data was available for case D2. N.A.*, not applicable as CAA absent on these sections. An expanded Table listing all 16 cases can be found in the Supplementary data.

probable AD (Table 2). Both cases demonstrated an intense punctate labelling with [3H]-PIB (Fig. 1A and D) that was strongly associated with the cortical region, although there was also a sparse labelling extending into the immediate subcortical white matter (Fig. 1D, case A2). As demonstrated by the labelling reactions performed in the presence of cold competitor ligand (BTA-1, 10 μM) the vast majority of the binding signal in both the grey and white matter was fully displaceable (Fig. 1B and E).

Alignment of the autoradiography images with the 6E10 (Aβ) immunohistochemistry of the adjacent sections (Fig. 1C and F) indicated a substantial overlap with the punctate staining pattern observed with [3H]-PIB and that this extended across both the white and grey matter lesions. This low-magnification correlation was also confirmed by the higher magnification images (Fig. 1G, case A2). However, it is also clear from these images that there are some areas which although intensely labelled with [3H]-PIB display reduced 6E10 immunoreactivity and this may in part reflect the enhanced sensitivity of the autoradiography method.

Consistent with its known poor sensitivity for DPs (Dickson, 2005) Thioflavin S only strongly labelled the sparse CPs (and CAA) associated with this case (Fig. 1G). Nevertheless there was good correspondence between the radiotracer and all forms of Aβ pathology examined. The ability of [3H]-PIB to label DPs more intensely than Thioflavin S probably reflects the >100-fold higher affinity of radioligand for Aβ fibrils relative to the dye (Lockhart *et al.*, 2004). This dataset demonstrates that at typical tracer concentrations [3H]-PIB can bind not only CPs but also DPs.

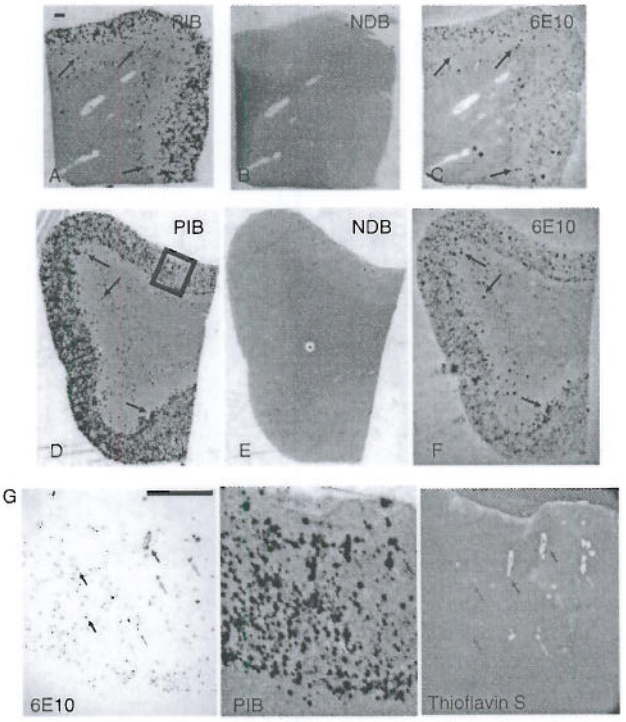


**Fig. 1** Images of adjacent MFG sections from two Category A pathology cases (A1 in **A–C**; A2 in **D–G**), showing correspondence of [3H]-PIB binding (**A** and **D**) with 6E10-immunoreactive Aβ deposits (**C** and **F**). NDB is demonstrated in sections treated with the non-radioactive competitive ligand BTA-1 (**B** and **E**). Black arrows demonstrate a number of specific corresponding features. Asterisks mark staining artefacts on 6E10 sections. Higher power representative images of boxed area from case A2 arranged in consecutive cryostat order (**G**). Selected corresponding pathological features are highlighted in pink (DPs), orange (CPs) and blue (CAA). Scale bar 1 mm.

## Category B sections [mixed pathology (DPs, CPs, CAA, NFTs)]

Sections from the SPL were pre-selected for the presence of all lesion types under investigation. The low-magnification images of sections labelling with [3H]-PIB were again very similar to those obtained with the MFG. A dense, punctate cortical staining pattern was observed (Fig. 2A and D) that was, in most instances, fully displaceable and which largely overlapped with the 6E10 labelled sections (Fig. 2C and F). Two features however differentiated these sections from the Category A cases (Fig. 1).

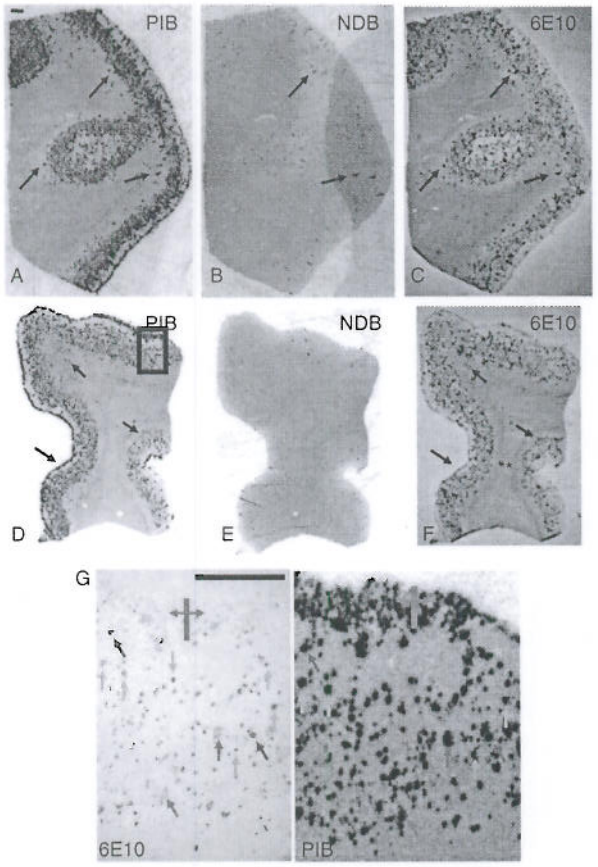


**Fig. 2** Images of adjacent SPL sections from two Category B pathology cases (B1 in **A**–**C**; B2 in **D**–**G**), showing correspondence of PIB binding (**A** and **D**) with 6E10-immunoreactive Aβ deposits (**C** and **F**). NDB is demonstrated in sections treated with the non-radioactive competitive ligand BTA-1 (**B** and **E**). Arrows demonstrate a number of specific corresponding features, including subpial diffuse amyloid deposits (black arrows on left of **D** and **F**). Note that on both sections a considerable number of PIB-labelled areas are not completely displaced by the cold BTA-1 compound and that these additionally coincide with 6E10-labelled foci (black arrows on B). Higher power representative images of boxed area from case B2 arranged in consecutive cryostat order (**G**). Selected corresponding pathological features are highlighted in pink (DPs), orange (CPs) and blue (CAA). The pink bar and arrows demonstrate corresponding staining of a subpial band of diffuse plaques. Scale bar 1 mm.

First, a number of radiolabelled foci were more obviously retained on the sections incubated with cold competitor ligand (Fig. 2B and E), which as discussed in the Category C cases coincided with CAA. Secondly, the intense labelling observed with [3H]-PIB along the cortical surface of case B2 (Fig. 2D) was associated with a band of weakly 6E10 immunoreactive material (Fig. 2F). Higher power images of the 6E10 sections indicated the presence of subpial 'band' or 'ribbon-like' Aβ diffuse deposits associated with the outer portion of the cortical molecular layer (layer 1) (Fig. 2G). The Aβ deposits in subpial lesions have been demonstrated to be diffuse, with only small amounts of amyloid fibrils present (Yamaguchi *et al.*, 1991). This finding reinforces our previous contention that PIB will also be sensitive *in vivo* to 'diffuse' deposits.

Although Gallyas staining revealed the presence of NFTs in both cases (Table 2) it was not possible to clearly assign any of the [3H]-PIB labelling with this pathological feature due to the high density, close proximity and greater size of the Aβ lesions. However, as demonstrated for the Category D cases [3H]-PIB clearly labels NFTs [see 'Category D sections (NFT-predominant pathology) section].

## Category C sections (CAA-predominant pathology)

The OCL is frequently and severely affected by cerebrovascular amyloid deposition in normal ageing and a range of neurodegenerative diseases such as AD (Attems, 2005). Sections labelled with [3H]-PIB from each of the cases displayed strong, punctate staining that at low magnification was broadly similar to the cortical patterns associated with the Category A and B cases (Fig. 3A and D). There was, however, a marked difference in the CAA labelling pattern in the presence of cold competitor ligand. While there was almost complete displacement of the radiolabel in case C1 (Fig. 3B), case C2 retained significant areas of radiolabel, although the overall intensity of the labelled structures was visibly reduced (Fig. 3E). Additional staining of adjacent sections with both 6E10 and Thioflavin S confirmed the presence of Aβ positive, amyloidotic blood vessels and that the foci of radiolabel retained after treatment with the cold competitor compound remained associated with these structures (Fig. 3G). These features are termed the CAA-associated non-displaceable binding (CAA-NDB).

Although the origins of the CAA-NDB cannot be fully addressed in this study, given the relatively small number of cases examined, one obvious difference between these two cases was their ApoE status. Cases C1 (CAA-NDB negative) and C2 (CAA-NDB positive) were ε2/ε3 and ε4/4, respectively. Both the remaining two category C cases were negative for CAA-NDB and possessed ε3/ε3 genotypes (see supplementary data Table). Across the remaining categories CAA pathology was present only in case A2 and cases B1-4. All of these CAA cases were positive for CAA-NDB and contained at least one ε4 allele. Although provocative, further detailed analysis is clearly required to understand the origins of the CAA-NDB.

## Category D sections (NFT-predominant pathology)

Hyperphosphorylated tau proteins, the major components of NFTs, are folded into an amyloid structure and thus have the potential to be labelled with [3H]-PIB. The ECX

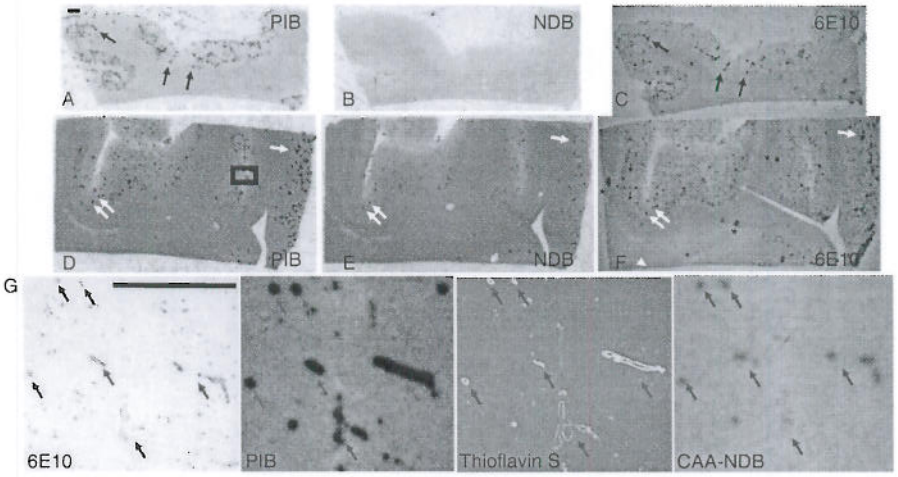


**Fig. 3** Images of adjacent OCL sections from two Category C pathology cases (C1 in **A**–**C**; C2 in **D**–**G**), showing correspondence of PIB binding (**A** and **D**) with 6E10-immunoreactive Aβ deposits (**C** and **F**). NDB is demonstrated in sections treated with the non-radioactive competitive ligand BTA-1 (**B** and **E**). Black arrows demonstrate a number of specific corresponding features. Asterisks mark staining artefacts on 6E10 sections. Note that associated with case C2 (**D**–**F**) the majority of the PIB-labelled areas are not completely displaced by the cold BTA-1 compound and that these additionally coincide with 6E10-labelled foci (black arrows on **E** and **F**). Higher power images of boxed area from case C2 arranged in consecutive cryostat order showing correspondence of PIB binding with 6E10-immunoreactive Aβ deposits, Thioflavin S-stained amyloid deposits and CAA-NDB (**G**). Blue arrows demonstrate a selection of corresponding amyloidotic blood vessels. Scale bar 1 mm.

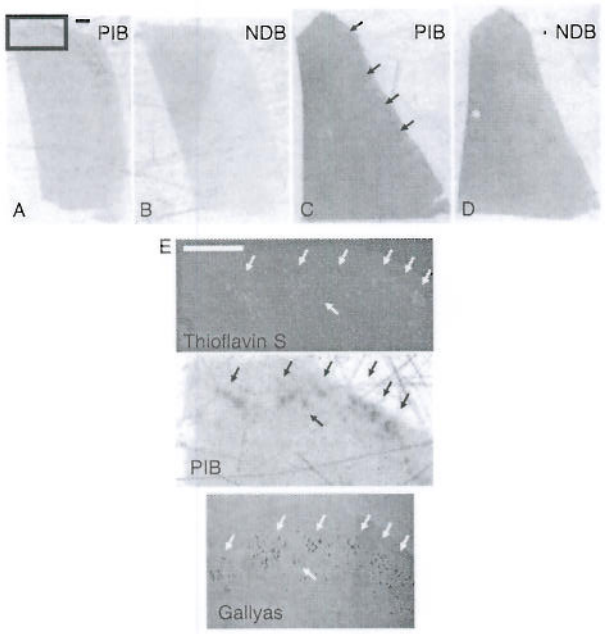


**Fig. 4** Representative images of adjacent ECX sections from Category D pathology cases (D1 **A**-**B** and D2 **C**-**D**) demonstrating specific binding of [3H]-PIB (**A** and **C**). NDB is demonstrated in sections treated with the non-radioactive competitive ligand BTA-1 (**B** and **D**). Higher power representative images of boxed area from case D1 arranged in consecutive cryostat order showing correspondence of PIB binding with Thioflavin S and Gallyas-positive NFT formations (**E**). White and black arrows demonstrate a selection of corresponding features. Scale bar 1 mm.

appears to be particularly susceptible to the formation of NFTs (Braak and Braak, 1992) and the cases associated with this category were pre-selected for their absence of Aβ pathology. Associated with case D1 a diffuse, interrupted band of PIB labelling was observed running along the superficial cortical layers (Fig. 4A). Incubation with cold competitor ligand demonstrated that the binding of [3H]-PIB to this lesion was fully displaceable (Fig. 4B). Consistent with its sparse pathological scoring for NFTs (Table 2), case D2 displayed a more discrete punctate labelling with [3H]-PIB that was again associated with the superficial cortical layers and fully displaceable (Fig. 4C and D).

Higher magnification images of the adjacent sections from case D1, labelled with Thioflavin S and Gallyas stains, confirmed the presence of an amyloid structure and NFTs, respectively, that were intimately associated with [3H]-PIB (Fig. 4E). The observed labelling pattern is consistent with localization of the radioligand to the 'stellate cell islands' found in the pre-alpha layer (layer II) of the ECX and that as this layer sweeps laterally the 'islands' disappears and are replaced by a non-interrupted neuronal band that plunges diagonally through the transentorhinal cortex (Braak and Braak, 1992). Excellent co-registration of individual NFTs with radiolabelled features was also observed in the high-power images of case D2 (see supplementary data Figure). These data indicate that [3H]-PIB can, at a very low concentration, label pathologic human amyloid deposits other than those containing fibrillar Aβ.

## Discussion

The data demonstrate for the first time that at tracer concentrations the neuroimaging agent PIB is not specific for CPs, one of the defining pathological features of AD, but that it additionally binds a range of Aβ containing lesions including DPs and CAA. The study also established that PIB decorates the tau containing amyloid structures associated with NFTs. However, the contribution of NFTs to the overall AD-associated PIB retention pattern is likely to be minor due to the much greater binding associated with Aβ lesions. Taken together these findings strongly suggest that *in vivo* [11C]-PIB cortical uptake primarily reflects Aβ-related cerebral amyloidosis (i.e. is a marker of all fibrillar Aβ containing pathology: DPs, CPs and CAA).

It is worth emphasising that the experimental protocols used in this study differ significantly from the previous studies investigating the interaction of PIB with human brain sections (Klunk *et al.*, 2003; Mathis *et al.*, 2003, 2004; Bacskai *et al.*, 2007) and that these may explain the novel findings associated with the current study. First, fresh, frozen brain sections were utilized in order to maintain the integrity of both the lesions and the surrounding tissue as close to *in vivo* as possible. Secondly, the use of autoradiography rather than fluorescence techniques permitted the use of concentrations (i.e. low nM range) relevant to *in vivo* imaging studies (Mathis *et al.*, 2004; Rowe *et al.*, 2007), with a detection method insensitive to potential tissue quenching and auto-fluorescence artefacts. Thirdly, detailed supporting histological staining was performed on adjacent sections allowing a direct correlation with the microscopic lesions.

## Relevance of findings to *in vivo* imaging studies using PIB

Translation of these findings provides a framework through which the disparities in PIB cortical uptake and neuropathology patterns can be re-evaluated. Plaque type appears to have only a minor influence on PIB binding, as both DPs and CPs are bound with high avidity. PIB uptake in areas with low CP density (e.g. the striatum) and the lack of increase in PIB binding associated with clinical disease progression may both be a consequence of PIB binding to DPs. Histopathological studies indicate that plaque load, a measure of both DPs and CPs, may be high in non-demented individuals (Bouras *et al.*, 1994). While CPs may increase with further overt disease progression, degradation and loss of CPs may also occur as late clinical stages are reached (Brun *et al.*, 1981, 1985; Wegiel *et al.*, 2001). Cortical uptake of PIB in PET is thus a faithful representation of the pathological data, i.e. widespread and dense SP deposition as an early, even preclinical, event in the pathogenesis of AD.

The presence of the CAA-NDB, in the subgroup of ε4 positive cases, highlights the importance of understanding the interaction of PIB with CAA, due to this fundamental difference in behaviour compared with SPs. Autopsy analysis of a 'PIB-positive' DLB case indicated that CAA was the major pathological source of amyloid and suggested that this lesion type can by itself be a major source of [11C]-PIB cortical uptake (Bacskai *et al.*, 2007). Furthermore, our findings are congruent with those from a study in which the presence of the ε4 allele was linked with a higher cortical uptake of [11C]-PIB, irrespective of clinical diagnosis (Rowe *et al.*, 2007). CAA is biochemically different to parenchymal SPs in that it is formed primarily from Aβ 1-40 fibrils, although this varies with neuroanatomical location (Attems, 2005). SPs are generally enriched in Aβ 1-42 species and are additionally subjected to a wide range of post-translational modifications, such as oxidation, isomerization and N-terminal truncation (Lockhart, 2006). Although, *in vitro* data indicates that the interaction of PIB with fibrils formed from either Aβ 1-40 or Aβ 1-42 is more or less identical (Klunk *et al.*, 2005) this does not rule the possibility that post-translation modifications may selectivity alter the interaction of PIB with one pool. Additionally, the observation that the CAA-NDB was not restricted to the OCL but that it was also observed in the SPL and MFG regions suggests that it is a generic feature. ApoE-ε4 is linked both with CAA severity (Alonzo *et al.*, 1998; Chalmers *et al.*, 2003) and conformation changes to amyloid structure (Sanan *et al.*, 1994), and these factors combined with biochemical differences in the Aβ pools may account for the occurrence of the CAA-NDB. The data strongly suggests that all individuals undergoing imaging scans with all classes of amyloid imaging probes should be genotyped for ApoE4 and stratified for potential differences in the patterns or kinetics of ligand retention.

The deposition of Aβ lesions is a common neuropathological finding in a number of conditions other than AD such as vascular dementia (Alonzo *et al.*, 1998) and DLB (Tsuboi *et al.*, 2005; Ballard *et al.*, 2006). The current study clearly supports the continued application of amyloid imaging as another clinical tool to identify and stratify dementias based on their cortical Aβ load (Rowe *et al.*, 2007; Rabinovici *et al.*, 2007). Although, the current study does not directly address the ability of PIB to act as a pharmacodynamic marker, for drugs targeting Aβ metabolism (Pangalos *et al.*, 2005), the data suggests that any change in the cortical uptake of the ligand cannot be ascribed to the appearance or disappearance of a particular Aβ lesion type.

It is reasonable to assume that the interaction between PIB and NFTs is due to the presence of high affinity binding sites associated with the amyloid fold of the tau, given that these structures can be labelled by the chemically related compounds Thioflavin S and T (Dickson, 2005). The weak labelling of the NFTs, relative to that observed with the Aβ lesions, is consistent with a much lower density of binding sites associated with this form of amyloid and that tangles, in contrast to Aβ lesions, are therefore unlikely

Lockhart A, Ye L, Judd DB, et al. Evidence for the presence of three distinct binding sites for the thioflavin T class of Alzheimer's disease PET imaging agents on beta -amyloid peptide fibrils. J Biol Chem 2004.

Lockhart A. Imaging Alzheimer's disease pathology: one target, many ligands. Drug Discov Today 2006; 11: 1093–9.

Markesbery WR, Schmitt FA, Kryscio RJ, Davis DG, Smith CD, Wekstein DR. Neuropathologic substrate of mild cognitive impairment. Arch Neurol 2006; 63: 38–46.

Mathis CA, Wang Y, Holt DP, Huang GF, Debnath ML, Klunk WE. Synthesis and evaluation of 11C-labeled 6-substituted 2-arylbenzothiazoles as amyloid imaging agents. J Med Chem 2003; 46: 2740–54.

Mathis CA, Wang Y, Klunk WE. Imaging beta-amyloid plaques and neurofibrillary tangles in the aging human brain. Curr Pharm Des 2004; 10: 1469–92.

Mintun MA, Larossa GN, Sheline YI, et al. [11C]PIB in a nondemented population: potential antecedent marker of Alzheimer disease. Neurology 2006; 67: 446–52.

Mirra SS, Heyman A, McKeel D, et al. The Consortium to Establish a Registry for Alzheimer's Disease (CERAD). Part II. Standardization of the neuropathologic assessment of Alzheimer's disease. Neurology 1991; 41: 479–86.

Mochizuki A, Peterson JW, Mufson EJ, Trapp BD. Amyloid load and neural elements in Alzheimer's disease and nondemented individuals with high amyloid plaque density. Exp Neurol 1996; 142: 89–102.

Mott RT, Hulette CM. Neuropathology of Alzheimer's disease. Neuroimaging Clin N Am 2005; 15: 755–65, ix.

Nordberg A. PET imaging of amyloid in Alzheimer's disease. Lancet Neurol 2004; 3: 519–27.

Pangalos MN, Jacobsen SJ, Reinhart PH. Disease modifying strategies for the treatment of Alzheimer's disease targeted at modulating levels of the beta-amyloid peptide. Biochem Soc Trans 2005; 33: 553–8.

Price JL, Morris JC. Tangles and plaques in nondemented aging and "preclinical" Alzheimer's disease. Ann Neurol 1999; 45: 358–68.

Rabinovici GD, Furst AJ, O'Neil JP, et al. 11C-PIB PET imaging in Alzheimer disease and frontotemporal lobar degeneration. Neurology 2007; 68: 1205–12.

Rowe CC, Ng S, Ackermann U, et al. Imaging beta-amyloid burden in aging and dementia. Neurology 2007; 68: 1718–25.

Sanan DA, Weisgraber KH, Russell SJ, et al. Apolipoprotein E associates with beta amyloid peptide of Alzheimer's disease to form novel monofibrils. Isoform apoE4 associates more efficiently than apoE3. J Clin Invest 1994; 94: 860–9.

Selkoe DJ, Schenk D. Alzheimer's disease: molecular understanding predicts amyloid-based therapeutics. Annu Rev Pharmacol Toxicol 2003; 43: 545–84.

Serpell LC. Alzheimer's amyloid fibrils: structure and assembly. Biochim Biophys Acta 2000; 1502: 16–30.

Shoghi-Jadid K, Small GW, Agdeppa ED, et al. Localization of neurofibrillary tangles and beta-amyloid plaques in the brains of living patients with Alzheimer disease. Am J Geriatr Psychiatry 2002; 10: 24–35.

Small GW, Kepe V, Ercoli LM, et al. PET of brain amyloid and tau in mild cognitive impairment. N Engl J Med 2006; 355: 2652–63.

Suenaga T, Hirano A, Llena JF, Yen SH, Dickson DW. Modified Bielschowsky stain and immunohistochemical studies on striatal plaques in Alzheimer's disease. Acta Neuropathol (Berl) 1990; 80: 280–6.

Tsuboi Y, Dickson DW. Dementia with Lewy bodies and Parkinson's disease with dementia: are they different? Parkinsonism Relat Disord 2005; 11 (Suppl 1): S47–S51.

Verhoeff NP, Wilson AA, Takeshita S, et al. In-vivo imaging of Alzheimer disease beta-amyloid with [11C]SB-13 PET. Am J Geriatr Psychiatry 2004; 12: 584–95.

Wegiel J, Bobinski M, Tarnawski M, et al. Shift from fibrillar to nonfibrillar Abeta deposits in the neocortex of subjects with Alzheimer disease. J Alzheimers Dis 2001; 3: 49–57.

Wisniewski HM, Bancher C, Barcikowska M, Wen GY, Currie J. Spectrum of morphological appearance of amyloid deposits in Alzheimer's disease. Acta Neuropathol (Berl) 1989; 78: 337–47.

Yamaguchi H, Nakazato Y, Yamazaki T, Shoji M, Kawarabayashi T, Hirai S. Subpial beta/A4 amyloid deposition occurs between astroglial processes in Alzheimer-type dementia. Neurosci Lett 1991; 123: 217–20.